Modeling of Discontinuities in General Coaxial Waveguide Structures by the FDTD-Method

Jan Van Hese, *Student Member, IEEE*, and Daniël De Zutter

Abstract—**The finite difference time domain (FDTD)-method is applied to model generalized coaxial waveguide structures with discontinuities. The cross-section of the waveguide consists of a closed outer conductor and one or two inner conductors of arbitrary shape. The cross-section can have any number of dielectric materials with losses. The singular field-behavior near sharp edges is explicitly included in the finite-difference scheme. Any kind of discontinuity can be handled: changes in cross-section as well as changes of material parameters. From the time-domain data, frequency-domain data (*S*-parameters) are obtained using Fourier-transform techniques.**

I. Introduction

IN HIGH-SPEED digital systems, the problem of interconnecting different sub-systems (on chip level or board level) forms a very important design topic. The accurate knowledge of the high-frequency behavior of typical discontinuities such as connectors and of other changes in the transmission path, becomes more and more important. However, the modeling of such structures is not an easy task. Due to the complexity and the diversity of the physical structures and the typical three-dimensional nature of the problem, only few of the classical modeling-techniques are suitable. In this paper we opt for the finite-difference time-domain (FDTD)-method [1] which was first proposed by K. S. Yee in 1966 and has been used extensively by many investigators to solve scattering [2], penetration and radiation [3], [4] and microstrip discontinuity problems [5], [6]. In this technique, the Maxwell time-dependent curl equations are solved using finite-difference techniques. In this paper we will use the method to model closed generalized coaxial waveguide structures with discontinuities. Fig. 1 shows a typical example of the physical structures under study. Using the FDTD-algorithm we typically get time-domain reflection and transmission data for an arbitrary input time-function, but it is possible to derive frequency domain data from these time-domain data using Fourier transform techniques [6].

In this paper, we present three examples. In a first example we analyse a simple test structure consisting of a straight coaxial waveguide-structure with a discontinuity that can be described as a change in impedance level. We compare the data obtained with our FDTD-implementation with theoretical results obtained with techniques used in classical circuit theory. In the second example, we examine the influence of a cylindrical bend on the propagation properties of a coaxial waveguide structure with rectangular cross-section. To do this we use an extension of the original FDTD-discretization scheme to cylindrical coordinates. This modified discretization scheme will be described in Section III. In the third example, we show the simulation results for the odd mode of a twinaxial transition structure consisting of two signal conductors with a continuous change in cross-section.

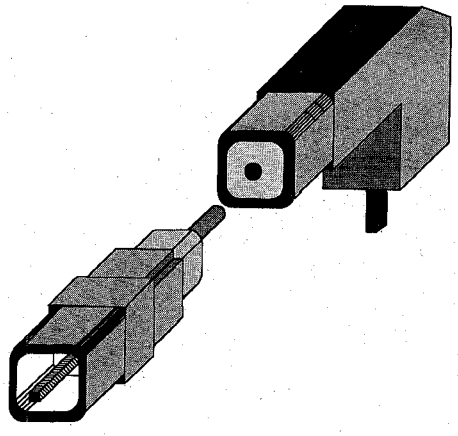

Fig. 1. Typical example of the physical structures under study.

II. Formulation of the Problem

We now give a more complete description of the type of physical structures we are focusing on in this paper. We are studying coaxial waveguide-structures. The cross-sections of the waveguide-structures consist of a closed outer conductor with an arbitrary shape, and one or two inner signal conductors also with an arbitrary shape (see Fig. 2). In the case of two inner signal conductors, the physical structure is assumed to be symmetrical, and the propagation of the even and odd mode can be simulated. In between the perfectly conducting inner and outer walls, different dielectric materials with losses can be present. In the direction of propagation, the structure can be straight or bent and can have all kinds of discontinuities such as changes in cross-section and/or in dielectric material.

In the sequel, the structure described above will be called the transition-section (see Fig. 3). In Fig. 3 this transition-section is located between the planes BB and

Manuscript received November 13, 1990; revised October 14, 1991.
The authors are with the Laboratory of Electromagnetism and Acoustics, University of Ghent, Sint-Pietersnieuwstraat 41, 9000-Ghent, Belgium.
IEEE Log Number 9105438.

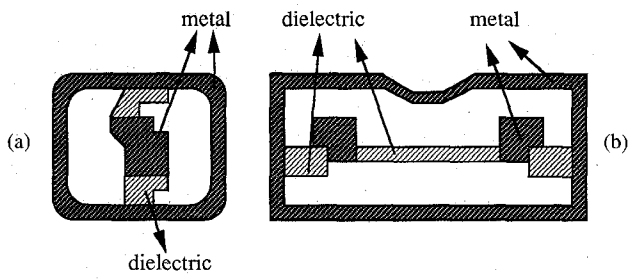

Fig. 2. Cross-sections of the waveguide structures under study. (a) Single signal conductor. (b) Two signal conductors.

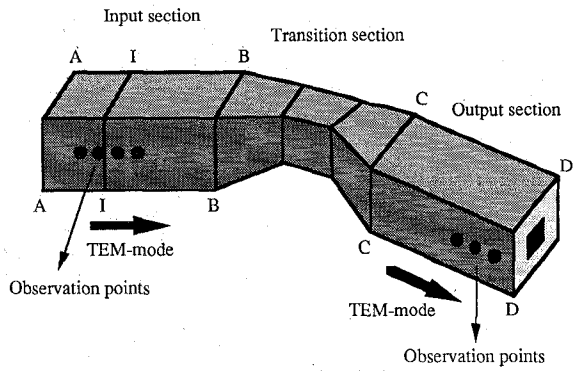

Fig. 3. Input-section, transition-section and output-section.

CC. In order to simulate the influence of this transition-section on signal propagation, we extend that section with an input-section between planes AA and BB and an output section between planes CC and DD. These sections are straight, semi-infinite and have a constant cross-section. The semi-infinite length is simulated using the so called 'absorbing boundaries' [7] at planes AA and DD. It is necessary to introduce these two sections because of the following reason. In the input-section we select an input plane (II in Fig. 3) where we inject a time-dependent input-field. The spatial distribution of this input-field over the cross-section of the input plane II is that of the basic TEM-mode supported by the input section. This input-field will propagate through the input-section towards the transition-section which contains the discontinuity we are investigating. Once the input-field reaches the discontinuity, reflections will occur. Due to the disturbance of the field-pattern in the cross-section, these reflections also contain higher order modes. This is also the case for the signal transmitted to the output-section. We propose to characterize the whole structure under study by examining the reflection and transmission in terms of the amplitude of the injected basic TEM-mode. Provided we make the input-section and output-section long enough, we will be able to find observation points (see Fig. 3) in the input-section and output-section (far enough from the discontinuities in the transition-section), where only the basic TEM-mode exists. In these observation points, the higher order modes generated by the transition will have vanished since these modes are excited below the cut-off frequency. This way of looking at the problem implies that the time-dependence of the input-field is such that the frequencies contained in it are lower than the cutoff frequency of the first higher order mode.

III. Application of the FDTD-Algorithm

1. FDTD Discretization Scheme in Cartesian and Cylindrical Coordinates

The formulation of the FDTD-solution method starts with the time-dependent Maxwell curl equations:

$$\mu_0 \frac{\partial \boldsymbol{h}(x, y, z)}{\partial t} = -\nabla \times \boldsymbol{e}(x, y, z, t)$$

$$\epsilon_0 \epsilon_r(x, y, z) \frac{\partial \boldsymbol{e}(x, y, z, t)}{\partial t} = \nabla \times \boldsymbol{h}(x, y, z, t) - \sigma(x, y, z)\, \boldsymbol{e}(x, y, z, t) \quad (1)$$

where μ_0 and ϵ_0 are the permeability and dielectric constant of vacuum and where $\epsilon_r(x, y, z)$ and $\sigma(x, y, z)$ are the relative dielectric constant and the conductivity of the material, which can both be a continuous function of the spatial coordinates x, y and z. We restrict ourselves to nonmagnetic materials.

The propagation of the input-field is simulated using finite-differences in the three different sections. In the input-section and the output-section, we use a discretization scheme in Cartesian coordinates. In the transition-section, we can either use a Cartesian coordinate system or a cylindrical coordinate system to describe the field propagation. The choice of the coordinate system depends on the shape of the discontinuity in the transition-section. The equations of the FDTD-discretization scheme in Cartesian coordinates are found in the classical way [1], [2] and are given in Appendix I. The discretization scheme in cylindrical coordinates is found in exactly the same way. We hereby start from the Maxwell time-dependent curl equations in cylindrical coordinates r, ϕ, x. The original Yee-unit cell in Cartesian coordinates [1], [2] is generalized as shown in Fig. 4. The FDTD-discretization equations in cylindrical coordinates are given in Appendix II. We will use the discretization scheme in cylindrical coordinates for our first example in which the influence of a cylindrical bend will be calculated.

It can be shown that the equations of the FDTD-discretization scheme satisfy the divergence equations $\nabla \cdot (\epsilon \boldsymbol{e}) = 0$ and $\nabla \cdot (\mu \boldsymbol{h}) = 0$ which is proven in Appendix III. Since we use a staggered grid in both the FDTD-discretization schemes (cylindrical and Cartesian), no spurious modes can occur as is stated in [8].

2. Connection of Discretization Schemes in Cartesian and Cylindrical Coordinates

In order to implement the simulation of a three-dimensional structure with a cylindrical bend as shown in Fig. 5, we need to derive a special transition formula at planes BB and CC which correctly connects the sections described in different coordinate systems [9]. The typical structure of Fig. 5 starts with an input section described in Cartesian coordinates, is followed by a corner section

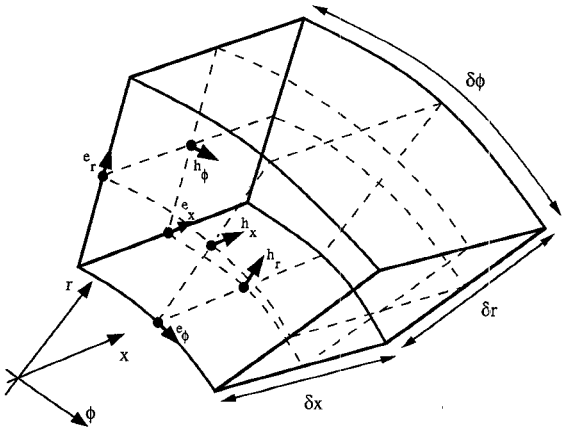

Fig. 4. Yee-unit cell in cylindrical coordinates.

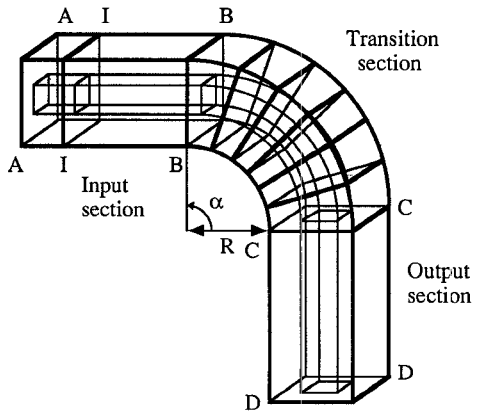

Fig. 5. Three dimensional structure with a cylindrical bend.

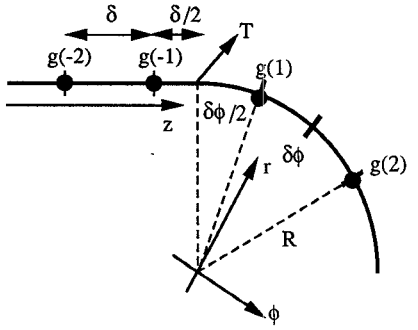

Fig. 6. Transition between the FDTD-scheme in Cartesian and cylindrical coordinates.

in cylindrical coordinates and ends with an output section again in Cartesian coordinates. The transition formula should not introduce any parasitical reflections, nor make the FDTD-scheme divergent. To obtain this, it is necessary to derive a transition formula which is at least of section order accuracy both in time and space.

To derive the transition formula, we focus on the situation shown in Fig. 6, which represents the transition between the scheme in Cartesian and cylindrical coordinates. The function g represents an arbitrary field-component. In the FDTD-discretization scheme, we typically need the derivative $[\partial g/\partial z](0)$. To evaluate this derivative at the transition point T, we expand the function values $g(-2)$ and $g(-1)$ (from the Cartesian coordinate system) and $g(1)$ and $g(2)$ (from the cylindrical coordinate system) as Taylor series centered around T:

$$g(-2) = g(0) - 3\,\delta z \frac{\partial g}{\partial z}(0) + 9\frac{\delta z^2}{2}\frac{\partial^2 g}{\partial z^2}(0) + O(\delta z^3)$$

$$g(-1) = g(0) - \delta z \frac{\partial g}{\partial z}(0) + \frac{\delta z^2}{2}\frac{\partial^2 g}{\partial z^2}(0) + O(\delta z^3)$$

$$g(1) = g(0) + \delta\phi \frac{\partial g}{\partial \phi}(0) + \frac{\delta\phi}{2}\frac{\partial^2 g}{\partial \phi^2}(0) + O(\delta\phi^3)$$

$$g(1) = g(0) + 3\,\delta\phi \frac{\partial g}{\partial \phi}(0) + 9\frac{\delta\phi}{2}\frac{\partial^2 g}{\partial \phi^2}(0) + O(\delta\phi^3) \tag{2}$$

After elimination of the second order derivatives $[\partial^2 g/\partial z^2](0)$, $[\partial^2 g/\partial\phi^2](0)$ and of $g(0)$ (this value is usually not known in the finite-difference scheme) from the equations in (2), we obtain the following expression for the first order derivative of g:

$$\frac{\partial g}{\partial z}(0) = \frac{9g(1) - 9g(-1) - g(2) + g(-2)}{3(\delta z + R\,\delta\phi)} + O(\delta z^2, \delta\sigma\phi^2) \tag{3}$$

Notice that the resulting formula is of second order accuracy in both δz and $\delta\phi$. This is the general formula that is applied to connect the meshes in Cartesian and cylindrical coordinates. The applicability of this formula is demonstrated in example 1 presented in Section V below.

3. *Input-Field Distribution and its Time-Dependence*

As explained before, the input-field distribution which is injected in the input-section is chosen to be the basic TEM-mode of the cross-section. This mode is calculated using a special purpose capacitance program which was developed to calculate the capacitance of arbitrary shaped two dimensional structures. The capacitance program, which basically uses an integral equation technique combined with point-matching, calculates the charge density on the conductors in the two dimensional cross-section. This approach was extensively checked [7]. Details will be presented in a forthcoming publication. Knowing the charge density distribution, it is possible to calculate the amplitudes of the transverse field-components of the TEM-mode. The time-dependence of the input-field is arbitrary but subjected to the restrictions mentioned at the end of Section II. In the examples, we have used a Gaussian time-dependence.

4. *Absorbing Boundary Conditions*

The input-section and output-section we added to the physical structure are semi-infinite straight waveguide structures. Since the FDTD-method is basically a discretization method, only a limited simulation space can be taken into account. Therefore, we have to simulate the

infinite length of input-section and output-section. This is done using so called absorbing boundary conditions [10] at the planes AA and DD in Fig. 3. In our applications, we can use first order boundary conditions because we know by construction the direction of the incident wave at the boundaries AA and DD. Let us focus on the input-section. Only TEM-waves going in the direction from BB to AA have to be absorbed at AA. In the sequel this direction will be indicated as the $(-z)$-direction. The propagation of a mode $f(x, y, z, t)$ travelling in the $(-z)$-direction satisfies (4) in each (x, y)-plane:

$$\left(\frac{\partial}{\partial z} - \frac{1}{v}\frac{\partial}{\partial t}\right) f(x, y, z, t) = 0. \tag{4}$$

In (4) v is the propagation speed of the considered mode in the input section. If the input-section is homogeneously filled with a medium with a relative dielectric constant ϵ_r then v is given by $c_0/\sqrt{\epsilon_r}$ where c_0 is the free-space velocity of light. Using the classical approximating finite-difference equations for the time and spatial derivatives [2], and using linear interpolation formulas, we obtain the following discrete approximating formulas for the transverse electric field-components:

$$e_x^{n+1}(i + 0.5, j, 1) = e_x^n(i + 0.5, j, 2) + \frac{v\,\delta t - \delta}{v\,\delta t + \delta} \cdot [e_x^{n+1}(i + 0.5, j, 2) - e_x^n(i + 0.5, j, 1)] \tag{5}$$

$$e_y^{n+1}(i, j + 0.5, 1) = e_y^n(i, j + 0.5, 2) + \frac{v\,\delta t - \delta}{v\,\delta t + \delta} \cdot [e_y^{n+1}(i, j + 0.5, 2) - e_y^n(i, j + 0.5, 1)]. \tag{6}$$

The implementation of (5) and (6) simulates the absorbing boundary at plane AA of the input-section. Similar equations are used to simulate the infinite length of the output-section.

5. *Influence of Singular Field-Behavior*

To improve the accuracy of the finite-difference scheme in structures with cross-sections with sharp metallic edges, we explicitly introduce the influence of the singularities in the FDTD-scheme. This is done by imposing special formulas in the calculation of the field-components near the sharp edges. Suppose we have a metallic edge as shown in Fig. 7. The metal conductor is aligned with the grid. Hence we can impose the boundary condition at the perfect conductor by requiring the tangential electric field-components at the boundary to be zero. However, for field-components in the direct vicinity of the sharp edges, another approach has to be followed [11]. To derive the formulas to calculate the h_x- and h_y-field components in the neighborhood of P shown in Fig. 7, we start from the Laurent series expansions of the h_x-, h_y-, and e_z-field components [12]. These Laurent series expansions (which include the singular behavior) are substituted in the Maxwell curl equations. Only the leading terms are taken into account. As a result, we obtain the following equations which determine the h_x- and h_y-field components near the sharp edge:

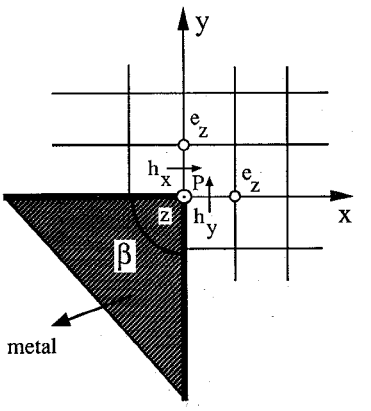

Fig. 7. Singularities of the electromagnetic field near sharp edges.

$$h_x^{n+0.5}(i, j + 0.5, k + 0.5) = h_x^{n-0.5}(i, j + 0.5, k + 0.5) - \frac{\delta t}{\mu_0\,\delta} v 2^{1-v} e_z^n(i, j + 1, k + 0.5) + \frac{\delta t}{\mu_0\,\delta}[e_y^n(i, j + 0.5, k + 1) - e_y^n(k, j + 0.5, k)] \tag{7}$$

$$h_y^{n+0.5}(i + 0.5, j, k + 0.5) = h_y^{n-0.5}(i + 0.5, j, k + 0.5) + \frac{\delta t}{\mu_0\,\delta} v 2^{1-v} e_z^n(i + 1, j, k + 0.5) + \frac{\delta t}{\mu_0\,\delta}[e_x^n(i + 0.5, j, k) - e_x^n(i + 0.5, j, k + 1)] \tag{8}$$

In (7) and (8), v takes the value $2/3$ if $\beta = 90°$. Comparing (7) and (8) with the original discretized equations (A4) and (A5) from Appendix I leads to the conclusion that the new equations (7) and (8) are obtained by introducing a singularity factor $v2^{1-v}$ [11].

6. *Evaluating the Simulation Results, Mode Amplitudes, Propagated Power*

To obtain the amplitude of the basic propagating TEM-mode as a function of time in the input-section and output-section, the following procedure is followed. We calculate the propagated power in the observation planes in the input-section and output-section as a function of time. This is done by integrating Poynting's vector over the entire cross-section. If we assume that in the observation points only the basic TEM-mode is propagating (see Sec-

tion II), the amplitude of this TEM-mode is proportional to the square root of the propagated power. By normalizing the obtained amplitude data to the maximum amplitude of the incident signal we finally get the results as presented in the following section.

IV. Numerical Examples

In this section three examples are presented. The first one is a simple waveguide filled with a dielectric material over a certain length. This example is used to demonstrate the accuracy of our method by comparing the numerically obtained S-parameters with their analytical values. The second example, a cylindrically bent coaxial waveguide structure, illustrates both the ability to deal with cylindrical coordinates and with non-disturbing transitions between cylindrical and Cartesian coordinates. The last example, a twinaxial transition section between signal conductors with rectangular cross-section and circular cross-section, illustrates the capability of our approach to deal with complex geometries.

1. Test Example: Filled Rectangular Waveguide

The geometry of this example is that of a rectangular TEM-waveguide, where we introduce a section of finite length with a different dielectric constant. Fig. 8 shows the geometry of the waveguide (a) and its cross-section (b). We have chosen this example because it allows us to compare the results obtained with the implemented FDTD-program and theoretically obtained results. To do this we first calculate the reflection and transmission responses in the time-domain using a Gaussian input-field time-dependence with a width of 30 ps. We define the width of the Gaussian to be the 5% width i.e., 0.05 times its maximum value. These time-domain results are shown in Fig. 9. From these time-domain results, we calculate the S-parameters as a function of frequency, using fast Fourier transform techniques. The amplitude of S_{11} and S_{21} are plotted up to 70 GHz. These S-parameters can also be calculated directly using the classical techniques of circuit theory. In this case we model the waveguide structure of Fig. 8 as a cascade of transmission lines, with the same impedances and electrical lengths as the different sections of the waveguide structure itself. The resulting S-parameters can be expressed as a function of the impedances Z_0, Z_1 of the different cross-sections and the propagation delay τ of the section filled with dielectric material using the formulas:

$$|S_{11}(f)|^2 = \frac{\left(\frac{Z_0}{Z_1} - \frac{Z_1}{Z_0}\right)^2 \sin^2(2\pi f\tau)}{4 + \left(\frac{Z_0}{Z_1} - \frac{Z_1}{Z_0}\right)^2 \sin^2(2\pi f\tau)}$$

$$|S_{21}(f)|^2 = 1 - |S_{11}(f)|^2 \tag{9}$$

In our case, we have to insert the following values which we got from our capacitance program [7]: $Z_0 = 27.60\ \Omega$, $Z_1 = 19.52\ \Omega$ and $\tau = 19.79$ ps. The theoretically calculated S-parameters are shown in dashed lines on Fig. 10 and are compared with the S-parameters obtained using the time-domain data (full lines). We see that there is an excellent agreement up to 60 GHz.

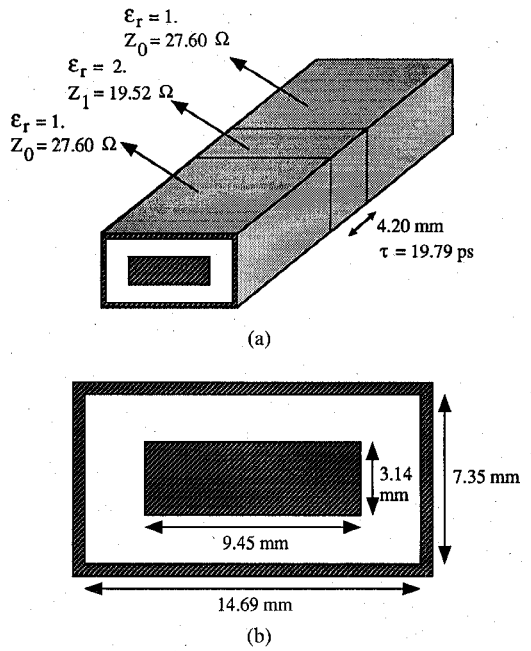

Fig. 8. (a) Test example. (b) Cross-section of the test example.

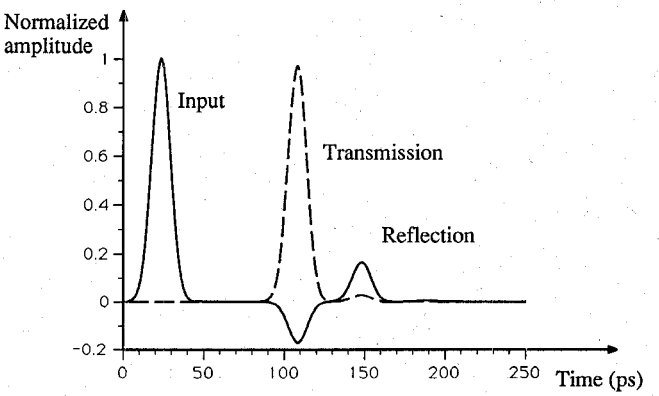

Fig. 9. Amplitude of the input-field and the reflected field in the input-section and of the transmitted field in the output-section for the structure of Fig. 8.

2. Cylindrically Bent Structure

As a second example, we give the simulation results for the cylindrically bent coaxial waveguide of Fig. 5. The input-field has a Gaussian time-dependence with a width of 60 ps. The dimensions of the coaxial cross-section are: outer conductor with height $8\ \delta = 6.66$ mm and width $10\ \delta = 8.33$ mm; inner conductor with height $4\ \delta = 3.33$ mm and width $6\ \delta = 5.00$ mm. The elementary spatial step $\delta = 0.833$ mm, the elementary time-step $\delta t = 1$ ps and the radius of the bend $R = 10$ mm. Fig. 11 shows the time-dependence of the amplitude of the basic

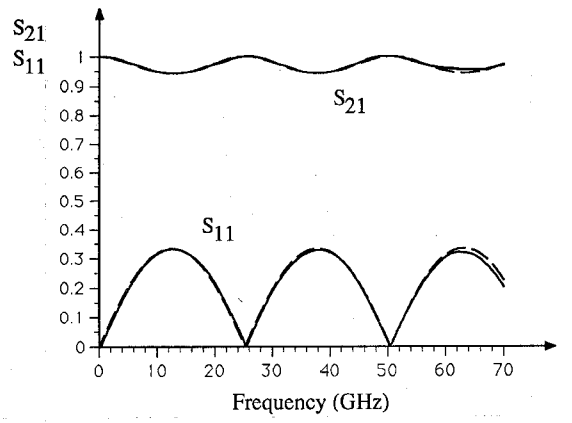

Fig. 10. *S*-parameters for the structure of Fig. 8; full lines: results obtained using the time-domain data of Fig. 9; dashed lines: analytical results.

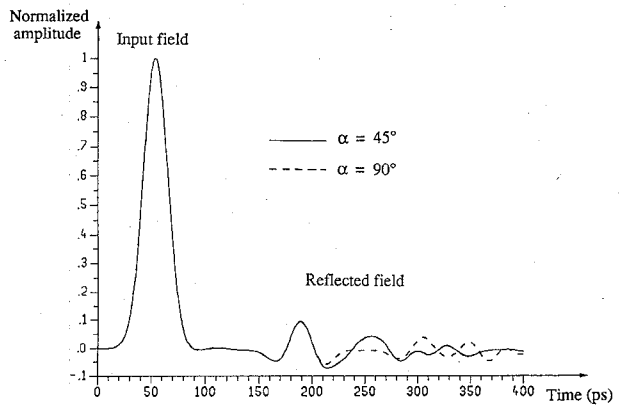

Fig. 11. Amplitude of the input-field and the reflected field in the input-section for $\alpha = 45°$ and 90°.

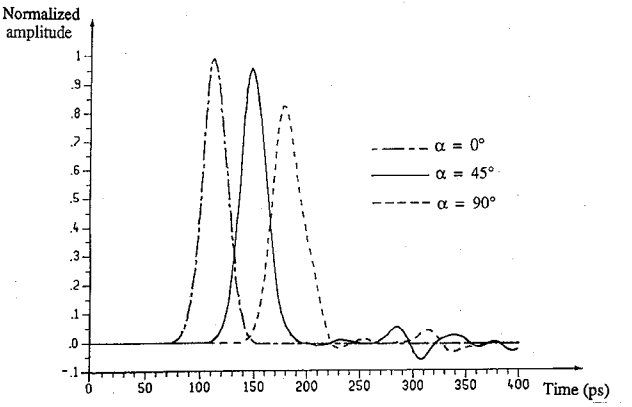

Fig. 12. Amplitude of the transmitted field in the output-section for $\alpha = 0°$, 45° and 90°.

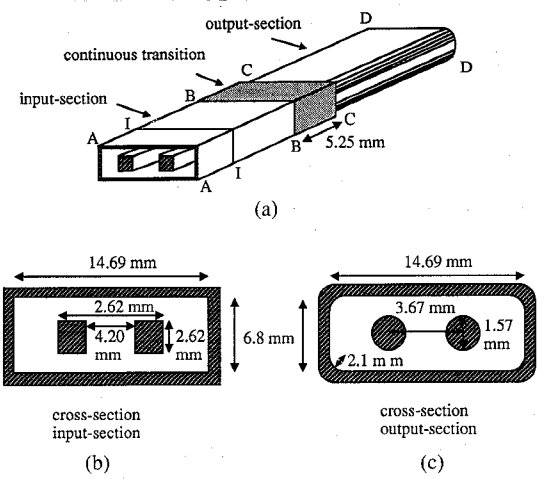

Fig. 13. (a) Twinaxial transition section, (b) cross-section at the input, (c) cross-section at the output.

TEM-mode in the input-section for two values of α: 45° and 90°. From 0 to 100 ps, the Gaussian input-field is seen, after 100 ps the reflected field appears. Fig. 12 shows the time-dependence of the amplitude of the basic TEM-mode in the output-section after transmission through the corner-section for three values of α: 0°, 45° and 90°. For $\alpha = 0°$ the input-field is transmitted without disturbance to the output-section. The cylindrical bend is perfectly described by the different sections. No approximations have to be made to describe the physical structure in the used coordinate systems. Taking more cells to discretize the coaxial structure is not necessary due to the fact that the singular field behavior near the sharp edges, where there is a strong concentration of the fields, is explicitely introduced in the FDTD-scheme. The authors thoroughly searched literature for other numerical or experimental data on coaxial bent waveguides. However, no suitable comparison material could be found. We invite the reader to critically examine the results given in this paper and to inform the authors about existing results that escaped our attention.

3. *Twinaxial Transition Section*

In the last example, we present the results for the symmetrical structure of Fig. 13(a). In the transition-section, we have a continuous change from the cross-section at the input section as shown in Fig. 13(b) to the cross-section at the output as shown in Fig. 13(c). The transition takes place over 10 elementary space steps i.e., 5.25 mm. The dimensions of the input-section and output-section are shown on the figures. The input-field has a Gaussian time-dependence with a 5% width of 40 ps. The elementary spatial step is equal to 0.262 mm; the elementary timestep is 0.5 ps. Fig. 14 shows the simulation results for the odd TEM-mode of the symmetrical waveguide. The full line in Fig. 14 shows the time-dependence of the injected input-field and the reflected field. The dashed line represents the field in transmission. In Fig. 15, we give density plots of Poynting's vector in the cross-section of the input-section (a) and of the output-section (b). These plots are made in regions in the structure where only the basic TEM-modes are propagating. In the density plots, the black areas in the centre represent the signal conductors where the propagated power is zero. The white areas represent maxima of the propagated power, i.e. a concentration of the field components. In Fig. 15(a), we clearly see the effect of the singular field-behavior near the sharp edges of the inner signal conductors. In Fig. 15(b), this effect is also seen as an unwanted effect caused by the

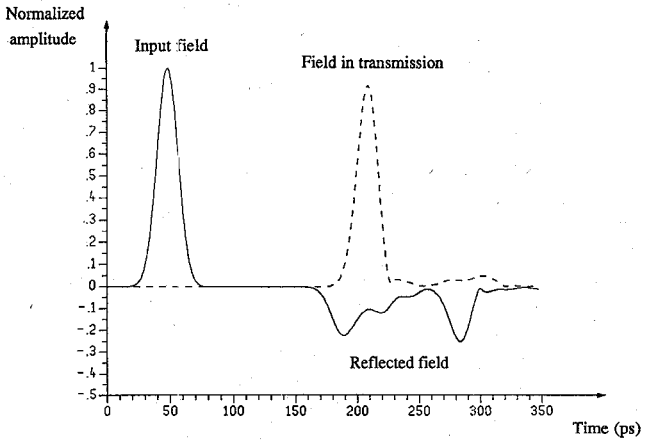

Fig. 14. Amplitude of the input-field, the reflected field and the transmitted field for the odd mode.

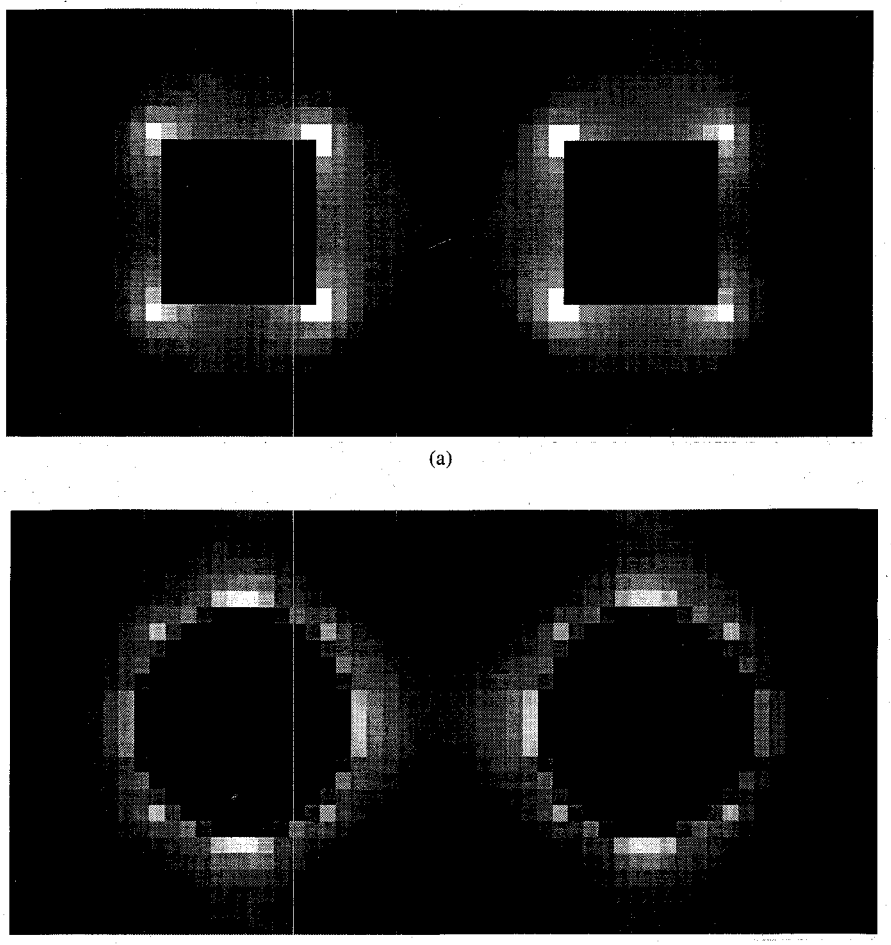

(a)

(b)

Fig. 15. Propagated power for the example of Fig. 13. (a) Cross-section at the input. (b) Cross-section at the output.

approximation of the circular signal conductors by the rectangular unit cells of the FDTD-scheme.

V. Conclusion

The FDTD-method can be used to model closed generalized coaxial waveguide structures with any kind and any number of discontinuities. The applicability of the method has been illustrated with three examples which show that our implementation of the FDTD-method is a powerful tool for modeling a great variety of structures.

Appendix I

The finite-difference equations in Cartesian coordinates are given by

$$
\begin{aligned}
&e_x^{n+1}(i+0.5,j,k)\\
&\quad=\left(1-\frac{\sigma(i+0.5,j,k)\,\delta t}{\epsilon_0\epsilon_r(i+0.5,j,k)}\right)e_x^n(i+0.5,j,k)\\
&\qquad+\frac{\delta t}{\epsilon_0\epsilon_r(i+0.5,j,k)\,\delta}\\
&\qquad\cdot[h_z^{n+0.5}(i+0.5,j+0.5,k)\\
&\qquad-h_z^{n+0.5}(i+0.5,j-0.5,k)\\
&\qquad+h_y^{n+0.5}(i+0.5,j,k-0.5)\\
&\qquad-h_y^{n+0.5}(i+0.5,j,k+0.5)] \qquad \text{(A1)}\\
&e_y^{n+1}(i,j+0.5,k)\\
&\quad=\left(1-\frac{\sigma(i,j+0.5,k)\,\delta t}{\epsilon_0\epsilon_r(i,j+0.5,k)}\right)e_y^n(i,j+0.5,k)\\
&\qquad+\frac{\delta t}{\epsilon_0\epsilon_r(i,j+0.5,k)\,\delta}\\
&\qquad\cdot[h_x^{n+0.5}(i,j+0.5,k+0.5)\\
&\qquad-h_x^{n+0.5}(i,j+0.5,k-0.5)\\
&\qquad+h_z^{n+0.5}(i-0.5,j+0.5,k)\\
&\qquad-h_z^{n+0.5}(i+0.5,j+0.5,k)] \qquad \text{(A2)}\\
&e_z^{n+1}(i,j,k+0.5)\\
&\quad=\left(1-\frac{\sigma(i,j,k+0.5)\,\delta t}{\epsilon_0\epsilon_r(i,j,k+0.5)}\right)e_z^n(i,j,k+0.5)\\
&\qquad+\frac{\delta t}{\epsilon_0\epsilon_r(i,j,k+0.5)\,\delta}\\
&\qquad\cdot[h_y^{n+0.5}(i+0.5,j,k+0.5)\\
&\qquad-h_y^{n+0.5}(i-0.5,j,k+0.5)\\
&\qquad+h_x^{n+0.5}(i,j-0.5,k+0.5)\\
&\qquad-h_x^{n+0.5}(i,j+0.5,k+0.5)] \qquad \text{(A3)}\\
&h_x^{n+0.5}(i,j+0.5,k+0.5)\\
&\quad=h_x^{n-0.5}(i,j+0.5,k+0.5)\\
&\qquad+\frac{\delta t}{\mu_0\,\delta}[e_y^n(i,j+0.5,k+1)\\
&\qquad-e_y^n(i,j+0.5,k)+e_z^n(i,j,k+0.5)\\
&\qquad-e_z^n(i,j+1,k+0.5)] \qquad \text{(A4)}\\
&h_y^{n+0.5}(i+0.5,j,k+0.5)\\
&\quad=h_y^{n-0.5}(i+0.5,j,k+0.5)\\
&\qquad+\frac{\delta t}{\mu_0\,\delta}[e_z^n(i+1,j,k+0.5)\\
&\qquad-e_z^n(i,j,k+0.5)+e_x^n(i+0.5,j,k)\\
&\qquad-e_x^n(i+0.5,j,k+1)] \qquad \text{(A5)}\\
&h_z^{n+0.5}(i+0.5,j+0.5,k)\\
&\quad=h_z^{n-0.5}(i+0.5,j+0.5,k)\\
&\qquad+\frac{\delta t}{\mu_0\,\delta}[e_x^n(i+0.5,j+1,k)\\
&\qquad-e_z^n(i+0.5,j,k)+e_y^n(i,j+0.5,k)\\
&\qquad-e_y^n(i+1,j+0.5,k)] \qquad \text{(A6)}
\end{aligned}
$$

where δt is the elementary time-step, δ is the elementary spatial step in the x-, y- and z-direction; $\sigma(i,j,k)$ and $\epsilon_r(i,j,k)$ are the conductivity and the relative dielectric constant of the material at coordinates $(i\,\delta, j\,\delta, k\,\delta)$.

Appendix II

The finite-difference equations in cylindrical coordinates are given by

$$
\begin{aligned}
&e_x^{n+1}(i+0.5,j,k)\\
&\quad=\left(1-\frac{\sigma(i+0.5,j,k)\,\delta t}{\epsilon_0\epsilon_r(i+0.5,j,k)}\right)e_x^n(i+0.5,j,k)\\
&\qquad+\frac{\delta t}{\epsilon_0\epsilon_r(i+0.5,j,k)}\left(\frac{1}{2r_j}+\frac{1}{\delta x}\right)\\
&\qquad\cdot h_\phi^{n+0.5}(i+0.5,j+0.5,k)\\
&\qquad+\frac{\delta t}{\epsilon_0\epsilon_r(i+0.5,j,k)}\left(\frac{1}{2r_j}-\frac{1}{\delta x}\right)\\
&\qquad\cdot h_\phi^{n+0.5}(i+0.5,j-0.5,k)\\
&\qquad+\frac{\delta t}{\epsilon_0\epsilon_r(i+0.5,j,k)\,r_j\,\delta\phi}\\
&\qquad\cdot[h_r^{n+0.5}(i+0.5,j,k-0.5)\\
&\qquad-h_r^{n+0.5}(i+0.5,j,k+0.5)] \qquad \text{(A7)}\\
&e_r^{n+1}(i,j+0.5,k)\\
&\quad=\left(1-\frac{\sigma(i,j+0.5,k)\,\delta t}{\epsilon_0\epsilon_r(i,j+0.5,k)}\right)e_r^n(i,j+0.5,k)\\
&\qquad+\frac{\delta t}{\epsilon_0\epsilon_r(i,j+0.5,k)\,r_{j+0.5}\,\delta\phi}\\
&\qquad\cdot[h_x^{n+0.5}(i,j+0.5,k+0.5)\\
&\qquad-h_x^{n+0.5}(i,j+0.5,k-0.5)]\\
&\qquad+\frac{\delta t}{\epsilon_0\epsilon_r(i,j+0.5,k)}[h_\phi^{n+0.5}(i-0.5,j+0.5,k)\\
&\qquad-h_\phi^{n+0.5}(i+0.5,j+0.5,k)] \qquad \text{(A8)}
\end{aligned}
$$

$$e_\phi^{n+1}(i, j, k + 0.5) = \left(1 - \frac{\sigma(i, j, k + 0.5)\,\delta t}{\epsilon_0\epsilon_r(i, j, k + 0.5)}\right) e_\phi^n(i, j, k + 0.5) + \frac{\delta t}{\epsilon_0\epsilon_r(i, j, k + 0.5)\,\delta x} \cdot [h_r^{n+0.5}(i + 0.5, j, k + 0.5) - h_r^{n+0.5}(i - 0.5, j, k + 0.5)] + \frac{\delta t}{\epsilon_0\epsilon_r(i, j, k + 0.5)\,\delta r} \cdot [h_x^{n+0.5}(i, j - 0.5, k + 0.5) - h_x^{n+0.5}(i, j + 0.5, k + 0.5)] \quad \text{(A9)}$$

$$h_x^{n+0.5}(i, j + 0.5, k + 0.5) = h_x^{n-0.5}(i, j + 0.5, k + 0.5) - \frac{\delta t}{\mu_0}\left(\frac{1}{2r_{j+0.5}} + \frac{1}{\delta r}\right) e_\phi^n(i, j, k + 0.5) + \frac{\delta t}{\mu_0}\left(\frac{1}{2r_{j+0.5}} - \frac{1}{\delta r}\right) e_\phi^n(i, j + 1, k + 0.5) + \frac{\delta t}{\mu_0\,\delta\phi r_{j+0.5}} [e_r^n(i, j + 0.5, k + 1) - e_r^n(i, j + 0.5, k)] \quad \text{(A10)}$$

$$h_r^{n+0.5}(i + 0.5, j, k + 0.5) = h_r^{n-0.5}(i + 0.5, j, k + 0.5) + \frac{\delta t}{\mu_0 r_j\,\delta\phi} [e_x^n(i + 0.5, j, k) - e_x^n(i + 0.5, j, k + 1)] + \frac{\delta t}{\mu_0\,\delta x} [e_\phi^n(i + 1, j, k + 0.5) - e_\phi^n(i, j, k + 0.5)] \quad \text{(A11)}$$

$$h_\phi^{n+0.5}(i + 0.5, j + 0.5, k) = h_\phi^{n-0.5}(i + 0.5, j + 0.5, k) + \frac{\delta t}{\mu_0\,\delta x} [e_r^n(i, j + 0.5, k) - e_r^n(i + 1, j + 0.5, k)] + \frac{\delta t}{\mu_0\,\delta r} [e_x^n(i + 0.5, j + 1, k) - e_x^n(i + 0.5, j, k)] \quad \text{(A12)}$$

where δt is the elementary time-step, δx, δr and $\delta\phi$ are the elementary spatial steps in the x-, r- and ϕ-direction (see Fig. 4); r_j is the distance from the bottom of cell (i, j, k) to the origin of the cylindrical coordinate system; $\sigma(i, j, k)$ and $\epsilon_r(i, j, k)$ are the conductivity and the relative dielectric constant of the material at coordinates $(i\,\delta x, j\,\delta r, k\,\delta\phi)$.

Appendix III

The solutions obtained with the FDTD-scheme satisfy the zero divergence constraints. To prove this we start from the Maxwell time-dependent curl equations (1) which lead to the FDTD-scheme if we introduce the following approximations for the partial derivatives. Let $f(x, y, z, t)$ be a general field component. After discretization, we denote:

$$f(i\,\delta, j\,\delta, k\,\delta, n\,\delta t) = f^n(i, j, k). \quad \text{(A13)}$$

In the FDTD-method, the derivatives are approximated by the second order finite-difference equations. For instance:

$$\frac{\partial}{\partial x} f(x, y, z, t) \rightarrow \frac{f^n(i + 0.5, j, k) - f^n(i - 0.5, j, k)}{\delta} = \Delta_x f^n(i, j, k) \quad \text{(A14)}$$

and

$$\frac{\partial}{\partial t} f(x, y, z, t) \rightarrow \frac{f^{n+0.5}(i, j, k) - f^{n-0.5}(i - 0.5, j, k)}{\delta t} = \Delta_t f^n(i, j, k) \quad \text{(A15)}$$

Using this notation we can write the finite-difference equations of the FDTD-scheme as

$$\Delta_t(\mu(h_x\boldsymbol{u}_x + h_y\boldsymbol{u}_y + h_z\boldsymbol{u}_z)) = -\Delta \times \boldsymbol{e} = -\begin{bmatrix} \boldsymbol{u}_x & \boldsymbol{u}_y & \boldsymbol{u}_z \\ \Delta_x & \Delta_y & \Delta_z \\ e_x & e_y & e_z \end{bmatrix} \quad \text{(A16)}$$

and

$$\Delta_t(\epsilon(e_x\boldsymbol{u}_x + e_y\boldsymbol{u}_y + e_z\boldsymbol{u}_z)) = \Delta \times \boldsymbol{h} = \begin{bmatrix} \boldsymbol{u}_x & \boldsymbol{u}_y & \boldsymbol{u}_z \\ \Delta_x & \Delta_y & \Delta_z \\ h_x & h_y & h_z \end{bmatrix} \quad \text{(A17)}$$

We now prove that the solutions obtained with (A16) and (A17) satisfy the discrete divergence equations:

$$\Delta \cdot (\epsilon\boldsymbol{e}) = \Delta_x(\epsilon e_x) + \Delta_y(\epsilon e_y) + \Delta_z(\epsilon e_z) = 0 \quad \text{(A18)}$$

and

$$\Delta \cdot (\mu \boldsymbol{h}) = \Delta_x(\mu h_x) + \Delta_y(\mu h_y) + \Delta_z(\mu h_z) = 0. \tag{A19}$$

We start for instance from (A16)

$$\mu_0 \, \Delta_t \boldsymbol{h} = -\Delta \times \boldsymbol{e} \tag{A20}$$

and let the Δ-operator work on both sides of (A20):

$$\mu_0 \, \Delta \cdot (\Delta_t \boldsymbol{h}) = -\Delta \cdot (\Delta \times \boldsymbol{e}) \tag{A21}$$

or

$$\begin{aligned} &\Delta \cdot (\Delta_t(\mu \boldsymbol{h})) \\ &\quad = -\Delta \cdot ((\Delta_y e_z - \Delta_z e_y)\boldsymbol{u}_x - (\Delta_x e_z - \Delta_z e_x)\boldsymbol{u}_y \\ &\qquad + (\Delta_x e_y - \Delta_y e_x)\boldsymbol{u}_z) \\ &\quad = -(\Delta_x \Delta_y e_z - \Delta_x \Delta_z e_y - \Delta_y \Delta_x e_z + \Delta_y \Delta_z e_x \\ &\qquad + \Delta_z \Delta_x e_y - \Delta_z \Delta_y e_x). \end{aligned} \tag{A22}$$

It can be easily checked that we can exchange the Δ-operators. If we do this we get from (A22) that

$$\Delta_t(\Delta \cdot (\mu \boldsymbol{h})) = 0 \tag{A23}$$

which means that

$$\Delta \cdot (\mu \boldsymbol{h}) \tag{A24}$$

is constant as a function of time. Since at the beginning of the simulation, all field components are identical to zero, we have proven that

$$\Delta \cdot (\mu \boldsymbol{h}) = 0. \tag{A25}$$

In a similar way, starting from (A17), we can prove that

$$\Delta \cdot (\epsilon \boldsymbol{e}) = 0 \tag{A26}$$

References

[1] K. S. Yee, "Numerical solutions of initial boundary value problems involving Maxwell's equations in isotropic media," *IEEE Trans. Antennas Propagat.*, vol. AP-14, pp. 302–307, May 1966.

[2] A. Taflove and M. E. Brodwin, "Numerical solution of steady-state electromagnetic scattering problems using the time-dependent Maxwell's equations," *IEEE Trans. Microwave Theory Tech.*, vol. MTT-23, pp. 623–630, Aug. 1975.

[3] A. Taflove, "Application of the finite-difference time-domain method to sinusoidal steady-state electromagnetic-penetration problems," *IEEE Trans. Electromagn. Compat.*, vol. EMC-22, pp. 191–202, Aug. 1980.

[4] A. Taflove and M. E. Brodwin, "Computation of the electromagnetic fields and induced temperatures within a model of the microwave-irradiated human eye," *IEEE Trans. Microwave Theory Tech.*, vol. MTT-23, pp. 888–896, Nov. 1975.

[5] X. Zhang, J. Fang, K. K. Mei, and Y. Liu, "Calculations of the dispersive characteristics of Microstrip by the time-domain finite-difference method," *IEEE Trans. Microwave Theory Tech.*, vol. MTT-36, pp. 263–267, Feb. 1988.

[6] X. Zhang and K. K. Mei, "Time-domain finite-difference approach to the calculation of frequency-dependent characteristics of microstrip discontinuities," *IEEE Trans. Microwave Theory Tech.*, vol. 36, pp. 1775–1787, Dec. 1988.

[7] J. Van Hese, "Analyses and measurement methods for impedance controlled transition structures in high-speed systems" (in Dutch), *IWONL*, aanvraag, 1989.

[8] D. R. Lynch and K. D. Paulsen, "Origin of vector parasites in numerical Maxwell solutions," *IEEE Trans. Microwave Theory Tech.*, vol. 39, pp. 383–394, Mar. 1991.

[9] J. Van Hese and D. De Zutter, "Application of the FDTD method in the modeling of coaxial structures with discontinuities," in *1990 IEEE Antennas and Propagation Symp. Dig.*, Dallas, TX, May 7–11, pp. 1636–1639.

[10] G. Mur, "Absorbing boundary conditions for the finite-difference approximation of the time-domain electromagnetic-field equations," *IEEE Trans. Electromagn. Compat.*, vol. EMC-23, pp. 377–382, Nov. 1981.

[11] G. Mur, "The modeling of singularities in the finite-difference approximation of the time-domain electromagnetic-field equations," *IEEE Trans. Microwave Theory Tech.*, vol. MTT-29, pp. 1073–1077, Oct. 1981.

[12] D. S. Jones, *The Theory of Electromagnetism*. Oxford, England: Pergamon, 1964, pp. 566.

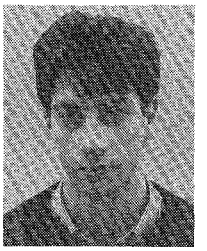

Jan Van Hese (S'91) was born in St-Niklaas, Belgium, on May 6, 1965. He received the degree in electrical engineering from the University of Ghent in 1988. He is currently working toward the Ph.D. degree in electrical engineering at the same university. His research concerns the electromagnetic modeling of high-frequency connectors.

Daniël De Zutter was born in Eeklo, Belgium, on November 8, 1953. He received the degree in electrical engineering from the University of Ghent in July 1976.

From September 1976 to September 1984 he was a Research and Teaching Assistant in the Laboratory of Electromagnetism and Acoustics (LEA) at the same university. In October 1981 he obtained the Ph.D. degree there and in the spring of 1984 he completed a thesis leading to a degree equivalent to the French Aggrégation or the German Habilitation. He is now a Professor at Ghent University and Research Director at the National Science Foundation of Belgium. Most of his earlier scientific work dealt with the electrodynamics of moving media, with emphasis on the Doppler effect and Lorentz forces. His research now focuses on all aspects of circuit and electromagnetic modeling of high-speed and high-frequency interconnections.

In 1990 he was elected as a member of the Electromagnetics Society.